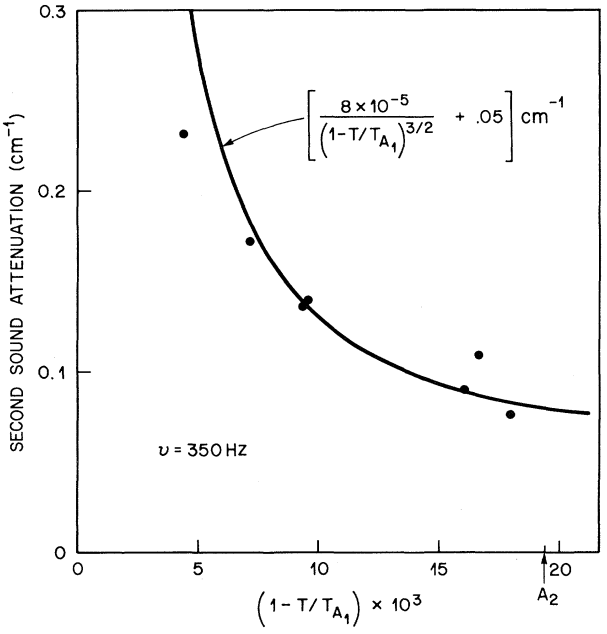

FIG. 3. Second-sound attenuation vs temperature. Solid curve is fit to data with use of temperature dependence predicted by Eq. (3) of text.

from Eq. (3) with use of the observed second-sound velocity. The attenuation increased with frequency, as expected, but the data did not permit a determination of the functional dependence on ω.

The authors wish to express their appreciation to M. C. Cross and M. Liu for illuminating discussions concerning these measurements, and to Wolfgang Sprenger for technical assistance.

[a]Permanent address: Physics Department, University of California, Davis, Cal. 95616.

[1]Mario Liu, Phys. Rev. Lett. 43, 1740 (1979). See also G. E. Gurgenishvili and G. A. Kharadze, Pis'ma Zh. Eksp. Teor. Fiz. 31, 593 (1980) [JETP Lett. (to be published)].

[2]K. Maki, Phys. Lett. 51A, 337 (1975); A. D. Gongadze, G. E. Gurgenishvili, and G. A. Kharadze, Zh. Eksp. Teor. Fiz. 75, 1504 (1978) [Sov. Phys. JETP 48, 759 (1978)].

[3]J. Wilks, *The Properties of Liquid and Solid Helium* (Clarendon, Oxford, England, 1967), p. 185.

[4]R. A. Sherlock and D. O. Edwards, Rev. Sci. Instrum. 41, 1603 (1970).

[5]Nuclepore Corp., 7035 Commerce Circle, Pleasanton, Cal. 94566.

[6]D. D. Osheroff and P. W. Anderson, Phys. Rev. Lett. 33, 686 (1974).

[7]W. P. Halperin, C. N. Archie, F. B. Rasmussen, T. A. Alvesalo, and R. C. Richardson, Phys. Rev. B 13, 2124 (1976).

[8]T. A. Alvesalo, T. Haavasoja, M. T. Manninen, and A. T. Soinne, Phys. Rev. Lett. 44, 1076 (1980).

[9]W. M. Saslow and C. R. Hu, to be published; M. Liu, to be published.

[10]M. A. Paalanen, private communication.

[11]Use of the leading edge of second-sound pulses for velocity determination is discussed by N. R. Brubaker, D. O. Edwards, R. D. Sarwinski, P. Seligmann, and R. A. Sherlock, J. Low Temp. Phys. 3, 619 (1970).

[12]The gyromagnetic ratio of ^{3}He is negative.

[13]K. Levin, Phys. Rev. Lett. 34, 1002 (1975).

[14]We do not contend Eq. (3) is applicable in ^{3}He-A_1. In our estimate of α_2, we have ignored the contribution from ζ_2, which can be calculated from the following works: P. Wölfle, J. Low Temp. Phys. 26, 659 (1977); P. Wölfle and D. Einzel, J. Low Temp. Phys. 32, 39 (1978).

Epitaxial Crystallization from a Melt: A Surface Molecular-Dynamics Study

Uzi Landman, Charles L. Cleveland, and Charles S. Brown
School of Physics, Georgia Institute of Technology, Atlanta, Georgia 30332
(Received 2 July 1980)

A surface molecular-dynamics method is described and employed to investigate the epitaxial crystallization of a supercooled melt. The procedure allows for thermal dissipation via a dynamic bulk reservoir, thus enabling the study of the approach to equilibrium. The early stages of the crystallization involve layering in the fluid, followed by intralayer ordering. The system evolution is described via layer profiles of particle number, temperature, potential energy, and orientational- and translational-order parameter versus time.

PACS numbers: 68.55.+b, 61.25.Bi, 61.50.Cj, 68.45.Da

We explore, by using a molecular-dynamics (MD) technique, the evolution, kinetics, and dynamics of an epitaxial-phase transformation.[1-4] In contrast with previous MD studies of the *equilibrium* properties of crystal surface-fluid systems in coexistence,[5] we study the *temporal evolution* and the *dynamics* of an initially *nonequilibrium* system. Prior to investigation of the liquid-

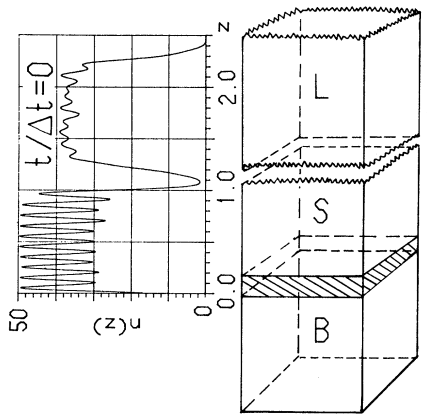

FIG. 1. Schematic description of the bulk (B), surface (S), liquid (L) system. The bulk block possesses 3D PBC's, the S and L possesses 2D PBC's. The coupling region is hatched. Also included is the particle number vs z profile of the system at $t=0$, consisting of an equilibrated surface and supercooled liquid film at $T^*=0.4$. Distance in units of 7.94σ.

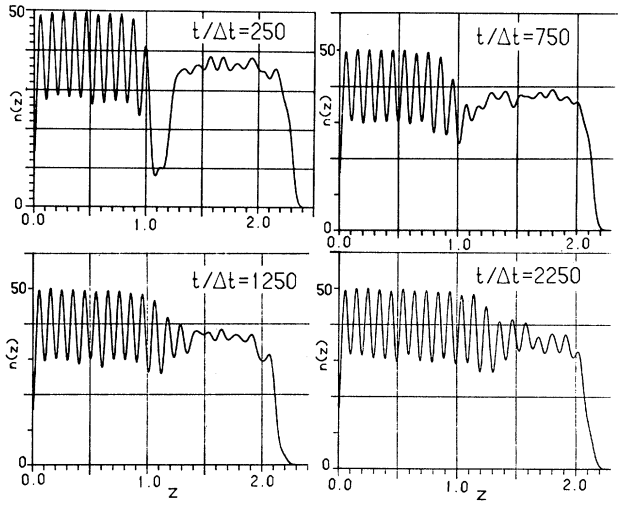

FIG. 2. Particle number vs z at four different times during the evolution of the system. Note the layering in the liquid region. The small peak at $z\simeq 1.1$, at the 250th time step corresponds to the embryonic cluster (see text).

solid interface we must first provide an adequate description of the substrate surface.

Surface Molecular Dynamics (SMD)—In MD the classical equations of motions of an interacting collection of particles are integrated and the recorded phase-space trajectories $[\vec{r}(t), \vec{v}(t)]$ are then analyzed. While periodic boundary conditions (PBC) are appropriate in most bulk MD studies the simulation of a semi-infinite system requires a special treatment. A schematic description of the system used by us is shown in Fig. 1. The "bulk block" (B) and "surface block" (S), consist each of 500 particles, interacting via a Lennard-Jones (L-J) 6-12 potential. The B system possesses three-dimensional (3D) PBC's and the S system possesses only 2D PBC's and is free in the z direction. Consequently, while the dynamics of particles in the S system is influenced by that of particles in the B system, the reverse statement does not hold (in the spirit of a bulk being an infinite reservoir whose dynamics and properties should not be influenced by surface effects). A region of the S system at the S-B interface is used as a "coupling region" on which we impose (time step by time step) a scaling of velocities such that the average kinetic energies (kinetic temperatures) in these layers are equal to the corresponding bulk ones. The thickness of this region (in this calculation three layers) is chosen to be larger than the pair interaction range to assure that the rest of the S system is not directly influenced by the bulk. The integration of the equations of motions is performed using a predictor-corrector method[6] with a time step[7] $\Delta t^*=0.0075$ and the evolution of the S and B systems is synchronized at each time step. The S-B system has been equilibrated as an fcc crystal (the density of the B system is adjusted to yield a vanishing average equilibrium pressure) exposing the (001) face, at a temperature $T^*=0.4$ (Ar melts at $T^*=0.7$). The above SMD technique has an advantage over slab configurations or calculations in which a static or a random matrix representation of the bulk are used. It allows the investigation of equilibrium and nonequilibrium surface and interface phenomena in which the dynamics of the bulk reservoir is included. Using our method, we currently investigate surface melting, defects, surface alloy dynamics, and transport phenomena.

Surface-Liquid System—Having equilibrated the surface described above, we prepare an equilibrated liquid sample. In the following we describe the results for a supercooled L-J liquid film (2D PBC's and free in the third direction) consisting of 500 particles, at $T^*=0.4$ (see block L in Fig. 1; other liquids such as liquid film at $T^*=0.737$ have also been investigated by us). Once equilibrated the L system is positioned at a distance chosen such that the smallest distance between a surface and a liquid particle is equal to 1.12σ (the location of minimum of the L-J poten-

tial) and the evolution of the coupled system is followed. (Note the initial absence of a temperature gradient.) Sample particle number versus z profiles at various time steps are shown in Fig. 2. It is observed that while the layers in the solid are well defined, those in the liquid fluctuate, averaging to the density profile of a liquid film. However, as time progresses a permanent layering of the liquid occurs. In fact, stratification of the liquid in the (001) direction (z direction) precedes the achievement of intralayer good crystalline order. Note also that the topmost layer of the surface (layer 10) first expands (in fact it is expanded already at $t=0$) and upon solidification of the liquid it contracts to the bulk spacing. In the following, layers in the liquid region are defined as regions in space whose thickness in the (001) direction is that of the next to the top-most layer of the solid surface (layer 9). Samples of the layer kinetic temperatures $T^* = k_B T/\epsilon$, defined as the mean kinetic energy of particles in layer l, and layer potential energies versus time are shown in Figs. 3 and 4. Also shown are the *orientational*-order parameters O_4 and O_6 defined as

$$O_m{}^l(t) = |N_l{}^{-1} \sum_{I,J \in l} N_{I,nn}{}^{-1} \exp(im\theta_{IJ})\,\Theta(R_{nn} - |\vec{r}_I - \vec{r}_J|)|^2, \quad m = 4, 6, \tag{1}$$

and the *layer translational* structure factors

$$S_l(\vec{k})/N_l = |N_l{}^{-1} \sum_{I \in l} \exp(i\vec{k}\cdot\vec{r}_I)|^2.$$

N_l is the number of particles in layer l at time t, Θ is the Heavyside step function, R_{nn} is the neighbor distance, $N_{I,nn}$ is the number of neighbors to particle I within a sphere of radius R_{nn}, θ_{IJ} is the "bond" angle between I and J with reference to an arbitrary direction. O_4 and O_6 take the values 1 and 0, respectively, for a perfect cubic crystal, while in the liquid state O_6 is generally larger than O_4. $\vec{k}$ is a bulk reciprocal-lattice vec-

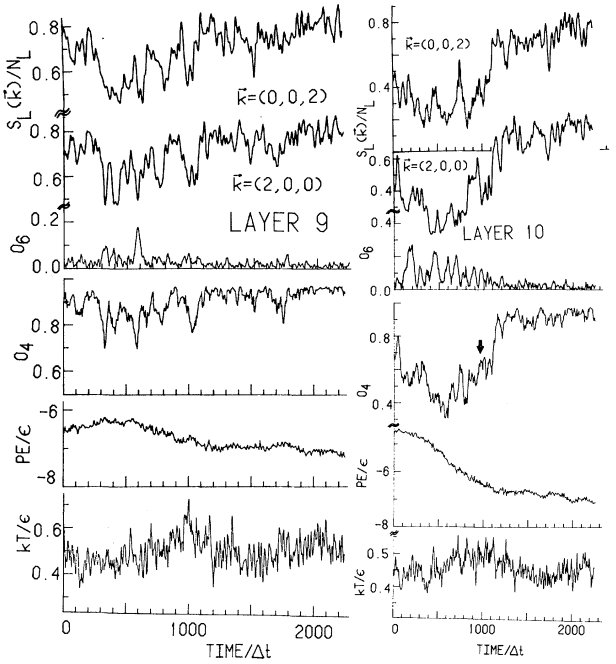

FIG. 3. Time evolution of the kinetic temperature $T^* = k_B T/\epsilon$, potential energy (PE), orientational-order parameters, O_4 and O_6, and structure factor $S_l(\vec{k})$, for layers 9 and 10. Note peaking of T^*, plateau in PE and increase in $S_l(0,0,2)$ at $t/\Delta t = 1000$, associated with layering in the solid. Order-disorder transformations in the layers are indicated by the behavior of O_4 and O_6. Compare positions of the arrowed peaks in O_4 and $S_l(2,0,0)$ which indicate intralayer ordering and dynamic coupling between layers.

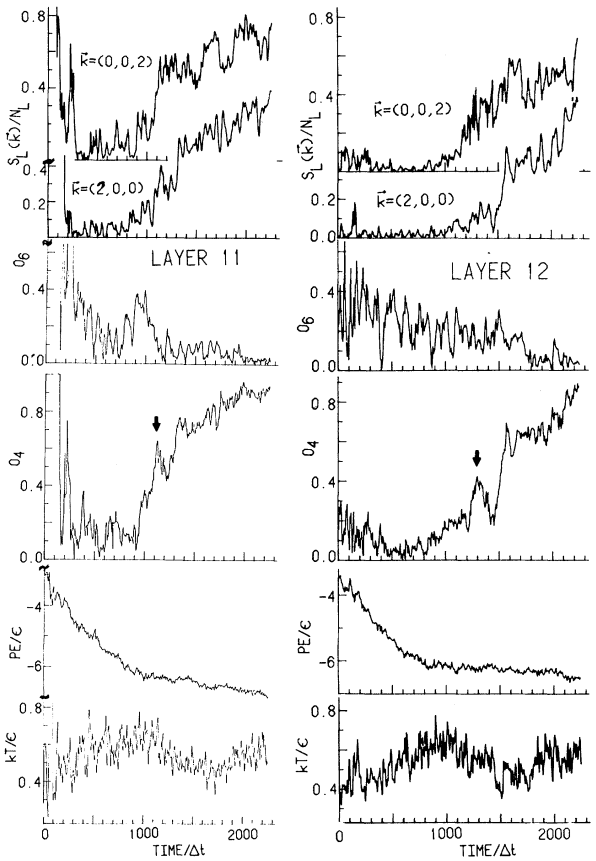

FIG. 4. Same as Fig. 3 for layers 11 and 12 (regions of crystallizing fluid).

tor.

The T^* plots undergo a maximum around $t/\Delta t = 1000$ for layers 9–14, when the monotonic decrease in the layers' potential energies achieve a plateau. In addition, the structure factors for $\vec{k} = (2\pi/a)\,(0, 0, 2)$, i.e., a reciprocal-lattice vector in the normal direction, exhibit a noted increase at this time. Notice that while at $t = 0$ layers 9 and 10 (solid surface) were less stable, less coordinated, than deeper layers they, along with the crystallized layers of the liquid, achieve eventually a bulk value (typically $S_l(\vec{k}) \gtrsim 0.8$). While the maximum in T^* indicates the expulsion of latent heat of ordering and is associated mainly with the "layering" of the fluid occuring at approximately the same time for a wide region of the liquid, the variations in O_4 and O_6 reflect intralayer ordering. Following the peak in O_4 designated by an arrow from layer to layer, it is seen that it shifts to longer times for higher layers. From the time delay of ordering in consecutive regions in the liquid the velocity of crystallization is estimated to be ~100 m/sec. Added confirmation that crystal-liquid layering precedes intralayer fcc crystalline ordering is provided via the $S_l(\vec{k})$'s for an in-plane reciprocal-lattice vector $\vec{k} = (2\pi/a)\,(2, 0, 0)$. It is also observed that layer 10 (and even 9) initially partially disorders (roughened?) and eventually orders (smoothed?).[8] The evolution of intralayer order (O_4, see Fig. 4 for layers 11 and 12) exhibits a sudden increase followed by a marked decrease, and finally an eventual rise. The decrease in order of a crystallizing layer is correlated with an increase in the order of the layer above it. Such systematic layer order-disorder transformations reflect strong dynamic and thermal interlayer coupling while little mass transport between layers is occurring. Increasing order in a layer induces ordering in a neighboring layer, with the expulsion of latent heat, which while dissipating partially disorders the first layer, delaying its eventual crystallization.

This new picture of epitaxial crystallization prompts a revision of current theoretical approaches[1-4] and demonstrates application of MD to temporal evolution of a nonequilibrium system.[9]

We gratefully acknowledge most valuable help and advice by Aneesur Rahman. The assistance and services of the Georgia Institute of Technology computer center staff, Rand Childs and Jerry Segers in particular, proved invaluable to this work. This work was supported by the U. S. Department of Energy under Contract No. EG-S-05-5489.

[1]D. P. Woodruff, *The Liquid State* (Cambridge Univ. Press, Cambridge, 1973), Chap. 8, and references therein.

[2]J. W. Cahn, Acta Metall. 8, 554 (1960).

[3]J. C. Brice, in *Current Topics in Materials Science*, edited by E. Kaldis and H. J. Scheel (North-Holland, Amsterdam, 1977), Vol. 2, p. 572, and references therein.

[4]H. Muller-Krumbhaar, in *Current Topics in Materials Science*, edited by E. Kaldis and H. J. Scheel (North-Holland, Amsterdam, 1977), p. 116; G. H. Gillmer and K. A. Jackson, *ibid.*, p. 80.

[5]J. Q. Broughton and F. F. Abraham, Chem. Phys. Lett. 71, 456 (1980); J. N. Cape and L. V. Woodcock, J. Chem. Phys. 73, 2420 (1980), and references therein.

[6]A. Rahman, Phys. Rev. 136, A405 (1964).

[7]Reduced units are used throughout the paper. The reduced time unit is $(\mu\sigma^2/\epsilon)^{1/2}$ where μ is mass, σ and ϵ are the Lennard-Jones 6-12 parameters. For argon $\sigma = 3.4$ Å, $\epsilon/k_B = 120$ °K, and the time unit is 1.65×10^{-12} sec. Energy is in units of ϵ. The potential cutoff is 2.5σ. In the figures, length is given in units of 7.94σ. Layers are numbered increasingly from the surface bulk interface, with layer 10 being the topmost layer of the solid surface. $t = 0$ is the time the equilibrated *B-S* and *L* systems are put together.

[8]In a case where the top surface layer contained a planer dislocation an annealing occured.

[9]See recent studies of homogeneous nucleation by C. S. Hsu and A. Rahman, J. Chem. Phys. 70, 5234 (1979), and 71, 4974 (1979).